

# Exploring the Temporal Consistency for Point-Level Weakly-Supervised Temporal Action Localization

Yunchuan Ma<sup>a</sup>, Laiyun Qing<sup>a,\*</sup>, Guorong Li<sup>a</sup>, Yuqing Liu<sup>a</sup>, Yuankai Qi<sup>b</sup>, Qingming Huang<sup>a</sup>

<sup>a</sup>University of Chinese Academy of Science, Beijing, 100190, China

<sup>b</sup>Macquarie University

---

## Abstract

Point-supervised Temporal Action Localization (PTAL) adopts a lightly frame-annotated paradigm (*i.e.*, labeling only a single frame per action instance) to train a model to effectively locate action instances within untrimmed videos. Most existing approaches design the task head of models with only a point-supervised snippet-level classification, without explicit modeling of understanding temporal relationships among frames of an action. However, understanding the temporal relationships of frames is crucial because it can help a model understand how an action is defined and therefore benefits localizing the full frames of an action. To this end, in this paper, we design a multi-task learning framework that fully utilizes point supervision to boost the model's temporal understanding capability for action localization. Specifically, we design three self-supervised temporal understanding tasks: (i) Action Completion, (ii) Action Order Understanding, and (iii) Action Regularity Understanding. These tasks help a model understand the temporal consistency of actions across videos. To the best of our knowledge, this is the first attempt to explicitly explore temporal consistency for point supervision action localization. Extensive experimental results on four benchmark datasets demonstrate the effectiveness of the proposed method compared to several state-of-the-art approaches.

**Keywords:** Point-Supervised Temporal Action Localization, Temporal Consistency, Self-Supervised Learning

---

\*Corresponding author

Email address: mayunchuan23@mailsucas.ac.cn (Yunchuan Ma)

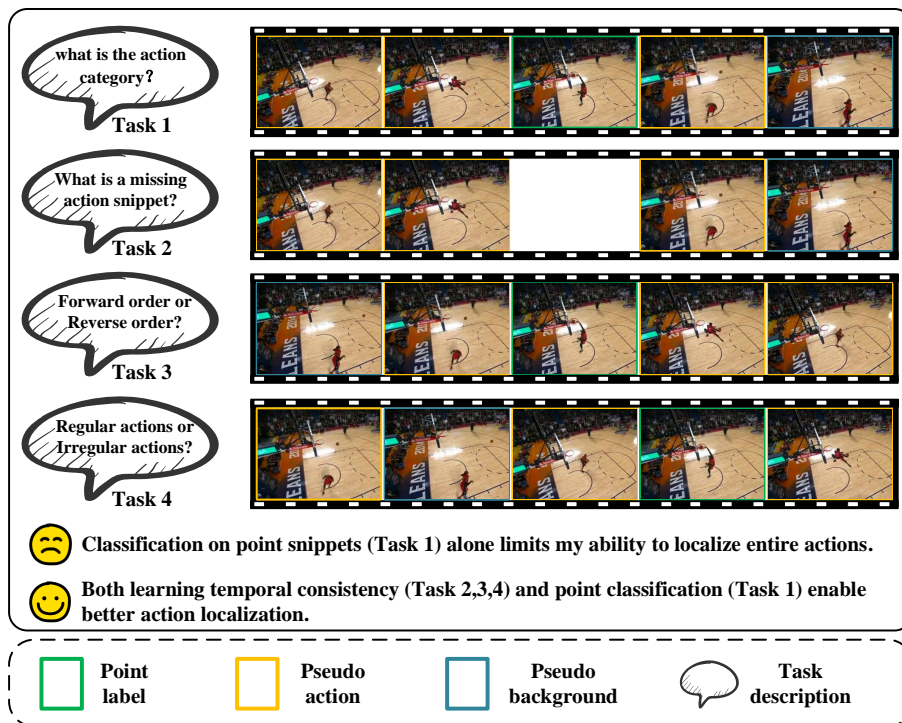


Figure 1: Previous methods primarily use point annotations to supervise the action classification of labeled snippets (Task 1). We improve upon this by incorporating three point-based self-supervised tasks (Tasks 2, 3, and 4) that enable the model to better capture temporal consistency and understand action sequences, thereby boosting action localization.

## 1. Introduction

Temporal action localization (TAL) plays a critical role in the video understanding field [1], aiming to predict the start and end timestamps of each action instance in the given untrimmed videos. Thanks to accurate action boundary labeling, conventional fully-supervised temporal action localization (FTAL) [2, 3] methods have achieved remarkable progress. Nevertheless, the frame-level annotation of action instances is laborious and time-consuming. To reduce the cost of annotating, researchers have increasingly turned to weakly-supervised temporal action localization (WTAL) [4, 5], which uses only video-level labels. Although significant progress has been made, its

performance remains limited due to the lack of fine-grained annotations.

To better balance annotation cost and model performance, point-supervised temporal action localization (PTAL) is proposed as a reliable solution, as it requires only one labeled frame per action instance without precise boundaries. As a pioneering method, SF-Net [6] employs an iterative strategy to mine pseudo action and background frames, thereby offering supplementary supervision throughout the training process. Subsequent research extends this paradigm by exploring effective strategies for leveraging such limited supervision. Typically, LACP [7] employs a greedy algorithm to generate a densely optimal sequence and leverages point annotations to learn the completeness of action instances. CRRC-Net [8] is proposed to further tackle intra-action variation and pseudo-label noise via co-supervised feature learning and probabilistic label mining. Recently, SNPR [9] proposes two neighbor-guided strategies to improve training efficiency and reduce label noise caused by sparse annotations and unreliable predictions.

Despite progress, the usage of point annotations of most existing methods remains limited to supervising snippet-level classification. Specifically, in a training process, an action locator relies on point annotations to supervise action classification at the snippet level and continuously mines pseudo-labels to enrich the supervisory information, as illustrated in **Task 1** of Figure 1. These methods neglect to explicitly model temporal relationships among frames of an action, which is crucial for models to understand the definition of an action. To tackle this problem, we introduce three self-supervised auxiliary tasks based on point annotations, as shown in **Tasks 2, 3, and 4** of Figure 1. These tasks facilitate the understanding of temporal relationships, which should be consistent across videos as long as they belong to the same action category. Specifically, the three point-based proxy tasks are as follows:

(i) **Action Completion (Figure 1 Task 2):** predicting the masked features of an annotated action snippet based on preceding and succeeding frames, thereby enabling the action locator to better model the temporal context of the action.

(ii) **Action Order Understanding (Figure 1 Task 3):** inferring whether an action sequence is temporally reversed, to strengthen the model’s awareness of action order.

(iii) **Action Regularity Understanding (Figure 1 Task 4):** determining whether

the action sequence is timely continuous, thus improving the model’s understanding of action regularities.

These three auxiliary tasks are jointly incorporated with the main task (*i.e.*, snippet classification) into a unified multi-task learning framework, which enables parallel training to strengthen temporal consistency modeling and boost action classification accuracy. Extensive experiments on four widely used datasets demonstrate the effectiveness of our method.

Our contributions are summarized as follows:

- We analyze the lack of temporal consistency modeling in current point-supervised methods and explore the benefits of temporal consistency modeling for action localization.
- We design three point-based self-supervised tasks: action completion, action order understanding, and action regularity understanding, to impose the capability of temporal consistency understanding on the base action detector.
- Extensive experimental results on four widely used datasets: THUMOS’14, GTEA, BEOID, and ActivityNet 1.3, show the effectiveness of the proposed method compared to several state-of-the-art methods.

## 2. Related Work

### 2.1. Temporal Action Localization

**Fully-Supervised Temporal Action Localization** relies on accurate annotations of action start and end timestamps, assigning precise action labels to every snippet in the training stage. This precise labeling leads to strong performance in both action classification and localization. Current approaches primarily include: (1) Proposal-based methods [10, 11], which generate temporal windows indicating action boundaries and refine these boundaries using regression modules. (2) Proposal-free methods [12], directly predict the probabilities for each snippet, with the snippet of highest probability selected as the action boundary proposal. Despite their excellent performance, these methods still face significant challenges due to the high cost of detailed labeling for each video snippet.

**Weakly-Supervised Temporal Action Localization** only provides video-level labels to localize action instances. Some studies adopt the multiple instance learning (MIL) mechanism to aggregate top-k snippet-level predictions into a video-level classification result. Some other works apply attention-based methods to boost detection performance. For example, UntrimmedNets [13] employs a soft attention mechanism to effectively retrieve relevant video segments. HAM-Net [14] proposes a hybrid attention mechanism encoding action completeness, while ASCN [15] similarly adopts hybrid attention integrated with frame differences to capture local contextual features. However, due to the unavailability of frame-level annotations, the performance of these models is significantly lower compared to fully-supervised methods.

**Point-Level Weakly-Supervised Temporal Action Localization** differs from traditional video-level Weakly-Supervised Temporal Action Localization in that it annotates a few numbers of action frames, *i.e.*, labeling only one single frame per action instance. The majority of approaches utilize point supervision to train action classifiers while also mining further reliable pseudo-labels to enhance supervisory information. As a typical example, LACP [7] generates pseudo-background annotations and jointly searches for the optimal sequence with point annotations to facilitate completeness learning. CRRC-Net [8] constructs and iteratively updates class-specific prototypes to achieve more reliable classification. To obtain more precise action instances, several studies perform additional boundary refinement on classification-generated proposals. TSPNet [16] leverages the human prior of annotating instance center regions to align proposal quality with confidence. HR-Pro [17] first learns discriminative snippet-level scores to generate reliable proposals, which are then refined using instance-level feature learning. However, existing methods primarily focus on snippet-level classification, neglecting the temporal consistency of action instances. Therefore, in this paper, we introduce three point-based self-supervised temporal learning tasks aimed at modeling the temporal consistency inherent in action instances.

## 2.2. Multi-Task Learning

Multi-task learning [18, 19, 20, 21] enhances task performance and model generalization through the joint learning of several related tasks, leveraging interaction

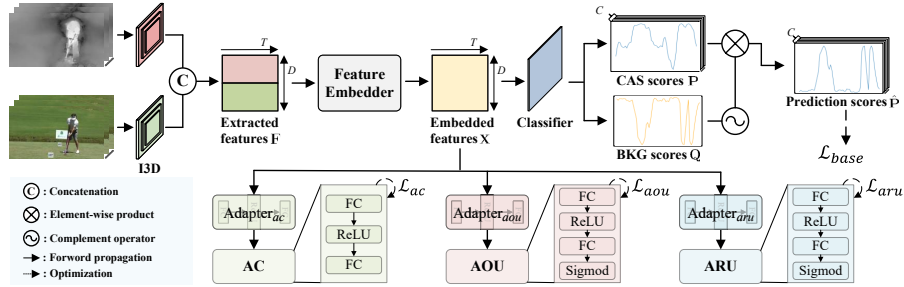


Figure 2: The workflow of the proposed method. The RGB and optical flow snippets of the input video are fed into the pretrained feature extractor to generate features  $\mathbf{F}$ , and are further embedded as  $\mathbf{X}$ . Besides the conventional snippet classification task, the embedded features  $\mathbf{X}$  are also used for joint training of the newly designed three temporal consistency tasks: Action Completion (AC), Action Order Understanding (AOU), and Action Regularity Understanding (ARU).

and information sharing among them. According to the degree of parameter sharing, multi-task learning methods can be broadly divided into two categories: hard parameter sharing and soft parameter sharing. In the hard parameter sharing strategy [18, 19], multiple tasks share the parameters in the encoder, while each task maintains an independent decoder to generate task-specific outputs. Unlike hard sharing, the soft parameter [20, 21] uses separate encoders for each task and shares information through task-interaction modules. In this paper, we adopt hard parameter sharing to jointly train the main task and self-supervised tasks, enhancing the model’s understanding of temporal consistency and its generalization.

### 3. Methodology

In this section, we first give the problem definition of P-TAL, our baseline architecture, as well as the baseline optimization loss in Sec. 3.1. Then, we introduce our multi-task learning setting in Sec. 3.2. Afterward, we present the details of our proposed three point-based self-supervised proxy tasks in Sec. 3.3. At last, we state the training and inference process in Sec. 3.4.

#### 3.1. Preliminaries

**Problem Definition.** In the point-level weakly-supervised temporal action localization setting, each action instance in the given training video is weakly annotated with a single timestamp  $t$  and its action category  $y$ , without providing temporal boundary information. The goal of this task is to learn an action locator from the sparse annotations  $P$ , which predict the instance  $(s, e, \hat{y}, c)$  of the input untrimmed video, where  $s$  and  $e$  indicate the start and end times of each action instance,  $\hat{y}$  denotes the predicted action category, and  $c$  represents the confidence score.

**Baseline Architecture.** The input video is initially split into  $T$  segments, each consisting of 16 frames. Next, following the previous approach [6, 7], we employ a pre-trained I3D model to extract RGB and optical flow features from each snippet, which are then concatenated along the channel dimension. The stacked snippet features can be represented  $\mathbf{F} \in \mathbb{R}^{T \times D}$ , where  $D$  is the dimension of each snippet-level feature. The extracted features are then fed into a feature embedding module to generate the embedded features  $\mathbf{X} \in \mathbb{R}^{T \times D}$ :

$$\mathbf{X} = \text{Embed}(\mathbf{F}) \quad (1)$$

The feature embedder includes two transformer encoder layers, followed by a 1D convolutional layer and ReLU activation. Afterward,  $\mathbf{X}$  is fed into a snippet-level classifier to generate class-specific activation sequence (CAS) scores  $\mathbf{P} \in \mathbb{R}^{T \times C}$  and the class-agnostic background scores  $\mathbf{Q} \in \mathbb{R}^T$ , where  $C$  is the number of action category and the classifier is composed of a 1D convolutional layer with the Sigmoid function. The final snippet-level predictions  $\hat{\mathbf{P}}$  can be computed by element-wise production:

$$\hat{\mathbf{P}} = \mathbf{P} \cdot (1 - \mathbf{Q}) \quad (2)$$

**Baseline Optimization Loss.** Since each action instance is labeled one point annotation and adjacent point annotations belong to separate action instances, we define pseudo-action snippets  $\mathcal{T}^+ = \{t_i\}_{i=1}^{N_{act}}$  and pseudo-background snippets  $\mathcal{T}^- = \{t_j\}_{j=1}^{N_{bkg}}$  using point annotations and the class-agnostic background scores, where  $N_{act}$  and  $N_{bkg}$  are the number of pseudo action snippets and background snippets, respectively. In specific, snippets located near a point annotation with lower class-agnostic background

scores than a specified threshold 0.1 are classified as pseudo-action snippets, which share the same action category as the point annotation. In contrast, snippets between two adjacent point annotations that either have the highest class-agnostic background score or exceed a given threshold of 0.95 are classified as pseudo-background snippets. The pseudo-action snippets are used for foreground supervision, formulated as:

$$\mathcal{L}_{cls}^{act} = \frac{1}{N_{act}} \sum_{c=1}^C \sum_{t \in \mathcal{F}^+}^{N_{act}} FL(\mathbf{P}_{t,c}) \quad (3)$$

Alternatively, pseudo-background snippets are used for background supervision:

$$\mathcal{L}_{cls}^{bkg} = \frac{1}{N_{bkg}} \sum_{t \in \mathcal{F}^-}^{N_{bkg}} FL(\mathbf{Q}_t) \quad (4)$$

$FL$  represents the focal loss function [22] as the same in [7]. In addition, a feature contrastive loss [23] is adopted to separate actions and background in the feature space. It can be formulated as:

$$\mathcal{L}_{contra} = -\frac{1}{C} \sum_{c=1}^C \sum_{t \in \mathcal{F}^+} \log \left( \frac{\exp(\tilde{\mathbf{X}}_t \cdot \tilde{\mathbf{m}}_c / \tau)}{\exp(\tilde{\mathbf{X}}_t \cdot \tilde{\mathbf{m}}_c / \tau) + \sum_{k \neq c} \exp(\tilde{\mathbf{X}}_t \cdot \tilde{\mathbf{m}}_k / \tau)} + \frac{\exp(\tilde{\mathbf{X}}_t \cdot \tilde{\mathbf{m}}_c / \tau)}{\exp(\tilde{\mathbf{X}}_t \cdot \tilde{\mathbf{m}}_c / \tau) + \sum_{t_j \in \mathcal{F}^-} \exp(\tilde{\mathbf{X}}_{t_j} \cdot \tilde{\mathbf{m}}_c / \tau)} \right) \quad (5)$$

where  $\mathbf{m}_c$  represents the prototype vector of the  $c$ -th action class, obtained by mean pooling the features of the  $c$ -th action snippets.  $\tau$  denotes the temperature parameter,  $\tilde{\mathbf{X}}$  denotes the L2 normalized features of  $\mathbf{X}$ .

In total, the baseline optimization loss can be expressed as:

$$\mathcal{L}_{base} = \lambda_1 \mathcal{L}_{cls}^{act} + \lambda_2 \mathcal{L}_{cls}^{bkg} + \lambda_3 \mathcal{L}_{contra} \quad (6)$$

where  $\lambda_1$ ,  $\lambda_2$ , and  $\lambda_3$  are the weighting parameters for  $\mathcal{L}_{cls}^{act}$ ,  $\mathcal{L}_{cls}^{bkg}$ , and  $\mathcal{L}_{contra}$ .

### 3.2. Multi-Task Learning Setting

To boost the temporal consistency of actions, we introduce three auxiliary tasks into the baseline, forming a unified multi-task learning framework. The overall multi-

task learning architecture is presented in Figure 2. Serving as shared features, the embedded features  $\mathbf{X}$  input to three task-specific adapters, each projecting them into a unique feature space:

$$\mathbf{X}^{ac} = \text{Adapter}_{ac}(\mathbf{X}) \quad (7)$$

$$\mathbf{X}^{aou} = \text{Adapter}_{aou}(\mathbf{X}) \quad (8)$$

$$\mathbf{X}^{aru} = \text{Adapter}_{aru}(\mathbf{X}) \quad (9)$$

Each adapter consists of a fully connected (FC) layer, a ReLU activation function, and another fully connected layer. Subsequently, the three task-specific features are fed into their corresponding task heads.

### 3.3. Point-based Self-Supervised Learning

We define the action localization branch in the upper part of Figure 2 as the main task (**Task 1**), while the three auxiliary task branches in the lower part of Figure 2 are denoted as **Tasks 2, 3, and 4**, respectively.

**Task2: Action Completion.** To improve the model’s temporal context awareness, we design a task inspired by BERT’s masked language model mechanism [24] in NLP, where the model learns to predict the feature representation of a labeled middle snippet based on its context. The labeled snippet is termed as  $\mathbf{X}_i^{ac}$ , and  $\mathbf{X}^{ac} = \{\mathbf{X}_i^{ac}\}_{i=1}^T$  represents the all  $T$  action completion task-specific features. We input the forward-left snippets  $\vec{\mathbf{S}}_i^{ac} = [\mathbf{X}_{i-t}^{ac}, \dots, \mathbf{X}_{i-1}^{ac}]$  and the backward-right snippets  $\overleftarrow{\mathbf{S}}_i^{ac} = [\mathbf{X}_{i+t}^{ac}, \dots, \mathbf{X}_{i+1}^{ac}]$  into our action completion task head  $H_{ac}$ :

$$\hat{\mathbf{X}}_i^{ac} = H_{ac}([\vec{\mathbf{S}}_i^{ac}, \overleftarrow{\mathbf{S}}_i^{ac}]) \quad (10)$$

where  $\hat{\mathbf{X}}_i^{ac}$  represents the predicted labeled snippet feature, and  $H_{ac}$  includes a fully connected layer, followed by a ReLU activation function and a subsequent fully connected layer. We calculate the cosine distance to evaluate the semantic gap between the

predicted results  $\hat{\mathbf{X}}_i^{ac}$  and the ground truth  $\mathbf{X}_i^{ac}$ :

$$\mathcal{L}_{ac} = 1 - \frac{1}{M} \sum_{j=1}^M \left( \frac{\mathbf{X}_j^{ac} \cdot \hat{\mathbf{X}}_j^{ac}}{\|\mathbf{X}_j^{ac}\|_2 \cdot \|\hat{\mathbf{X}}_j^{ac}\|_2} \right) \quad (11)$$

where  $M$  is the number of point-labels,  $\|\cdot\|_2$  represents the L2 normalized operation. The objective of this task is to minimize  $\mathcal{L}_{ac}$ .

**Task3: Action Order Understanding.** Learning the temporal action sequence order is effective in modeling temporal consistency of action instances. The goal of this task is to distinguish between forward and backward sequences. It motivates the model to capture more discriminative information about the order of temporal action sequences. We define the original forward sequence  $\vec{\mathbf{S}}_i^{aou} = [\mathbf{X}_{i-t}^{aou}, \dots, \mathbf{X}_i^{aou}, \dots, \mathbf{X}_{i+t}^{aou}]$  as a positive sample labeled 1, and its reversed version  $\overleftarrow{\mathbf{S}}_i^{aou} = [\mathbf{X}_{i+t}^{aou}, \dots, \mathbf{X}_i^{aou}, \dots, \mathbf{X}_{i-t}^{aou}]$  as a negative sample labeled 0. Next, both  $\vec{\mathbf{S}}_i^{aou}$  and  $\overleftarrow{\mathbf{S}}_i^{aou}$  are passed to the action order discriminator  $D_{aou}$ :

$$\overrightarrow{pred} = D_{aou}(\vec{\mathbf{S}}_i^{aou}) \quad (12)$$

$$\overleftarrow{pred} = D_{aou}(\overleftarrow{\mathbf{S}}_i^{aou}) \quad (13)$$

where the  $\overrightarrow{pred}$  and  $\overleftarrow{pred}$  represent the predicted results of  $\vec{\mathbf{S}}_i^{aou}$  and  $\overleftarrow{\mathbf{S}}_i^{aou}$ , respectively. This order discriminator  $D_{aou}$  architecture includes one fully connected layer, followed by a ReLU activation, another fully connected layer, and a Sigmoid function as the output. To encourage the model to capture the ordering of actions, we minimize the following loss function:

$$\mathcal{L}_{aou} = -\frac{1}{M} \sum_{j=1}^M [\log \overrightarrow{pred}_j + \log(1 - \overleftarrow{pred}_j)] \quad (14)$$

**Task4: Action Regularity Understanding.** Understanding the regularity of actions is crucial for temporal action detection. The purpose of this task is to distinguish between regular and irregular action sequences. It drives the model to focus on identifying key cues that reflect the regularity of temporal action sequences. We define the features

of regular action segments  $\bar{\mathbf{S}}_i^{aru} = [\mathbf{X}_{i-t}^{aru}, \dots, \mathbf{X}_i^{aru}, \dots, \mathbf{X}_{i+t}^{aru}]$  as positive samples with label 1, and create negative samples with label 0 by randomly shuffling the action order, such as  $\tilde{\mathbf{S}}_i^{aru} = [\mathbf{X}_{i-1}^{aru}, \mathbf{X}_{i+1}^{aru}, \mathbf{X}_i^{aru}, \mathbf{X}_{i-2}^{aru}, \mathbf{X}_{i+2}^{aru}]$ , when  $t$  are set to 2. Then,  $\bar{\mathbf{S}}_i^{aru}$  We then feed both  $\bar{\mathbf{S}}_i^{aru}$  and  $\tilde{\mathbf{S}}_i^{aru}$  into the action regularity discriminator  $D_{aru}$  to generate prediction scores  $\bar{pred}$  and  $\tilde{pred}$ :

$$\bar{pred} = D_{aru}(\bar{\mathbf{S}}_i^{aru}) \quad (15)$$

$$\tilde{pred} = D_{aru}(\tilde{\mathbf{S}}_i^{aru}) \quad (16)$$

$D_{aru}$  shares the same architecture as  $D_{aou}$ . We minimize the following loss function to help the model capture the inherent regularity of actions:

$$\mathcal{L}_{aru} = -\frac{1}{M} \sum_{j=1}^M [\log \bar{pred}_j + \log(1 - \tilde{pred}_j)] \quad (17)$$

### 3.4. Training and Inference

**Training.** The overall objective loss function is formulated as follows:

$$\mathcal{L}_{total} = \mathcal{L}_{base} + \lambda_{ac}\mathcal{L}_{ac} + \lambda_{aou}\mathcal{L}_{aou} + \lambda_{aru}\mathcal{L}_{aru} \quad (18)$$

where  $\lambda_{ac}$ ,  $\lambda_{aou}$ , and  $\lambda_{aru}$  are hyperparameters that control the trade-off between the auxiliary tasks.

**Inference.** During inference, we retain only the main branch trained with multi-task learning as the detector, without relying on the auxiliary task modules, to directly generate final prediction scores  $\hat{\mathbf{P}}$ . Then,  $\hat{\mathbf{P}}$  are processed into a series of proposals, and Soft-NMS [25] is employed to reduce overlap.

## 4. Experiment

### 4.1. Datasets and Evaluation

We conduct experiments on the four commonly-used temporal action localization datasets, including THUMOS14 [26], BEOID [27], GTEA [28], and ActivityNet1.3 [29].

**THUMOS’14** [26] serves as a challenging dataset for Temporal Action Localization, containing 413 untrimmed sports videos across 20 action categories. The average number of action instances per video is 15. The dataset is split into 200 videos for training and 213 videos for testing, as per the standard division.

**BEOID** [27] offers 58 video samples categorized into 34 operation classes across 6 different locations. It consists of 46 videos for training and 12 for testing.

**GTEA** [28] consists of 28 untrimmed videos capturing 7 fine-grained daily activities in a kitchen setting. We follow the standard split, using 21 videos for training and 7 for testing.

**ActivityNet 1.3** [29] includes 10,024 training videos, 4,926 validation videos, and 5,044 test videos, covering 200 action categories. On average, each video contains 1.6 action instances.

**Evaluation Metrics.** For a fair comparison, we evaluate the action localization performance on the four datasets using mean Average Precision (mAP) at various Intersection-over-Union (IoU) thresholds. If the generated proposal’s IoU exceeds the set IoU threshold and matches the correct category, it is regarded as a positive sample.

### 4.2. Implementation Details

To make a fair comparison, we follow the previous methods to split each video into non-overlapping 16-frame snippets and use a two-stream I3D [30] network pre-trained on Kinetics-400 as the feature extractor. The input feature dimension  $D$  is 2048, the adapter feature dimension is 512. We use the Adam optimizer with a learning rate of  $1e - 4$  and a weight decay of  $1e - 3$ , and set the batch size to 16 for model training. Empirically,  $\lambda_1$ ,  $\lambda_2$ ,  $\lambda_3$ ,  $\lambda_{ac}$ ,  $\lambda_{aou}$ , and  $\lambda_{aru}$  are 0.5, 1, 1, 0.5, 0.5, and 0.5, respectively. The temperature parameter  $\tau$  is 0.1, and each temporal window (*i.e.*, the temporal sequence composed of the labeled snippet and its surrounding snippets)

Table 1: Comparison with the state-of-the-art methods on THUMOS’14. We further compare our method with both fully-supervised and weakly-supervised approaches. For fairness, we adopt the same point annotations as used in [7]. Moreover, to enable a fair comparison with proposal-based two-stage methods [16, 17, 31], we also apply a proposal-based boundary adjustment similar to [17]. Results marked with † indicate our method with proposal-based refinement.

Supervision	Method	mAP@IoU (%)						AVG	AVG	AVG	
		0.1	0.2	0.3	0.4	0.5	0.6	0.7	(0.1:0.5)	(0.3:0.7)	(0.1:0.7)
Full supervised	TCANet [32] (CVPR’21)	-	-	60.6	53.2	44.6	36.8	26.7	-	44.3	-
	BMN+CSA [33] (ICCV’21)	-	-	64.4	58.0	49.2	38.2	27.8	-	47.5	-
	GCM [34] (TPAMI’21)	72.5	70.9	66.5	60.8	51.9	-	-	64.5	-	-
	VSGN [35] (ICCV’21)	-	-	66.7	60.4	52.4	41.0	30.4	-	50.2	-
	AFSD [36] (CVPR’21)	-	-	67.3	62.4	55.5	43.7	31.1	-	52.0	-
Weakly supervised	P-MIL [37] (CVPR’23)	71.8	67.5	58.9	49.0	40.0	27.1	15.1	57.4	38.0	47.0
	Zhou <i>et al.</i> [38] (CVPR’23)	74.0	69.4	60.7	51.8	42.7	26.2	13.1	59.7	38.9	48.3
	PivoTAL [39] (CVPR’23)	74.1	69.6	61.7	52.1	42.8	30.6	16.7	60.1	40.8	49.6
	ISSF [40] (AAAI’24)	72.4	66.9	58.4	49.7	41.8	25.5	12.8	57.8	37.6	46.8
	PVLR [41] (MM’2024)	74.9	69.9	61.4	53.1	45.1	30.5	17.1	60.9	-	50.3
	NoCo [42] (AAAI’2025)	75.2	70.7	63.0	54.1	44.0	31.7	17.7	61.4	42.1	50.9
Point supervised	ARST [43] (CVPR’19)	24.3	19.9	15.9	12.5	9.0	-	-	16.30	-	-
	SF-Net [6] (ECCV’20)	68.3	62.3	52.8	42.2	30.5	20.6	12.0	51.2	31.6	41.2
	LACP [7] (ICCV’21)	75.7	71.4	64.6	56.5	45.3	34.5	21.8	62.7	44.5	52.8
	BackTAL [44] (TPAMI’21)	-	-	54.4	45.5	36.3	26.2	14.8	-	35.4	-
	CRRC-Net [8] (TIP’22)	77.8	73.5	67.1	57.9	46.6	33.7	19.8	64.6	45.1	53.8
	SMBD [45] (ECCV’24)	-	-	66.0	57.9	47.0	36.0	22.0	64.2	45.7	-
	SNPR [9] (TIP’24)	77.9	73.9	66.6	59.4	48.6	36.7	22.7	65.3	46.8	55.1
	AAPL [46] (AAAI’25)	64.3	-	54.6	-	35.2	-	14.0	-	-	42.8
	<b>Ours</b>	<b>82.5</b>	<b>78.2</b>	<b>71.5</b>	<b>62.3</b>	<b>51.4</b>	<b>38.0</b>	<b>23.3</b>	<b>69.2</b>	<b>49.3</b>	<b>58.2</b>
	DCM [31] (ICCV’21)	72.3	64.7	58.2	47.1	35.9	23.0	12.8	55.6	35.4	44.9
	SF-Net+TSPNet [16] (CVPR’24)	75.5	-	57.9	-	33.1	-	12.3	-	-	44.8
	BackTAL+TSPNet [16] (CVPR’24)	77.1	-	63.5	-	43.4	-	19.7	-	-	51.7
	TSPNet [16] (CVPR’24)	82.3	77.6	70.1	60.0	49.4	37.6	24.5	67.9	48.3	57.4
	HR-Pro [17] (AAAI’24)	85.6	81.6	74.3	64.3	52.2	39.8	24.8	71.6	51.1	60.3
	QROT [47] (CVPR’25)	-	-	73.1	64.4	54.3	41.3	27.4	72.3	52.1	-
<b>Ours†</b>	<b>85.9</b>	<b>82.3</b>	<b>75.5</b>	<b>66.5</b>	<b>54.7</b>	<b>41.6</b>	<b>25.8</b>	<b>73.0</b>	<b>52.8</b>	<b>61.8</b>	

includes 5 snippet features. Our entire system is implemented using PyTorch, and all experiments are conducted on a single RTX-3090Ti GPU.

#### 4.3. Comparison with State-of-The-Art Methods

We evaluate our model’s performance and compared it with the latest PTAL methods, as well as some fully-supervised and weakly-supervised methods.

**THUMOS’14.** In Table 1, our method achieves the highest average mAP (0.1:0.7) 58.2% compared to all point-level and video-level weakly-supervised temporal action localization methods. In comparison to previous one-stage PTAL methods, the average mAP (0.1:0.7) of our method rises from 3.1% (Ours *v.s.* SNPR) to 17% (Ours *v.s.* SF-Net). Compared to the best-performing video-level weakly supervised method NoCo, our approach achieves a 7.3% higher score on the average mAP for IoU thresholds of 0.1:0.7. Our proposal-based refinement results also surpass other proposal-based PTAL methods, such as HR-Pro (61.8% *v.s.* 60.3%) and TSPNet (61.8% *v.s.* 57.4%). On the

Table 2: Comparisons of detection performance on GTEA, BEOID, and ActivityNet1.3 datasets. The symbol † indicates our results with boundary adjustment, following the same proposal-based refinement strategy as [17].

Method	GTEA					BEOID					ActivityNet1.3			
	mAP@IoU (%)					mAP@IoU (%)					mAP@IoU (%)			
	0.1	0.3	0.5	0.7	AVG[0.1:0.7]	0.1	0.3	0.5	0.7	AVG[0.1:0.7]	0.5	0.75	0.95	AVG[0.5:0.95]
SF-Net (ECCV'20)	58.0	37.9	19.3	11.9	31.0	62.9	40.6	16.7	3.5	30.9	-	-	-	-
LACP (ICCV'21)	63.9	55.7	33.9	<b>20.8</b>	43.5	76.9	61.4	42.7	25.1	51.8	40.4	24.6	5.7	25.1
CRRC-Net (TIP'22)	-	-	-	-	-	-	-	-	-	-	39.8	24.1	5.9	24.0
SMBD (ECCV'24)	75.0	61.3	41.1	14.2	47.4	<b>78.2</b>	71.0	52.5	25.2	57.4	-	-	-	-
SNPR (TIP'24)	74.3	62.8	35.7	13.7	46.6	77.2	64.3	44.0	24.5	53.1	41.3	<b>30.9</b>	4.8	<b>26.5</b>
AAPL (AAAI'25)	70.3	54.4	37.7	23.4	46.3	75.5	67.6	48.5	26.3	55.2	39.6	24.3	<b>5.6</b>	24.7
<b>Ours</b>	<b>76.6</b>	<b>64.3</b>	<b>45.3</b>	17.7	<b>50.3</b>	77.1	<b>72.1</b>	<b>55.7</b>	<b>28.4</b>	<b>60.2</b>	<b>42.3</b>	25.9	5.5	26.3
DCM (ICCV'21)	59.7	38.3	21.9	18.1	33.7	63.2	46.8	20.9	5.8	34.9	-	-	-	-
HR-Pro (AAAI'24)	72.6	61.1	37.3	17.5	47.3	78.5	72.1	55.3	26.1	59.4	42.8	<b>27.2</b>	<b>8.0</b>	27.1
TSP-Net (CVPR'24)	74.6	60.9	39.5	16.6	49.0	<b>83.8</b>	73.0	51.1	23.8	59.6	-	-	-	-
<b>Ours†</b>	<b>76.4</b>	<b>68.8</b>	<b>48.4</b>	<b>18.3</b>	<b>53.0</b>	79.5	<b>75.7</b>	<b>62.5</b>	<b>29.6</b>	<b>63.1</b>	<b>43.9</b>	27.1	5.6	<b>27.4</b>

Table 3: Quantitative results of different proxy tasks on the test split of THUMOS'14.

Proxy Task	AC		AOU		ARU	
Metric	Cos_Sim	Cos_Dist	AUC	ACC	AUC	ACC
	0.992	0.008	92.9%	85.7%	85.9%	77.4%

average mAP for IoU thresholds of 0.3:0.7, our method even outperforms certain fully-supervised approaches, such as ASFD (52.8% v.s. 52.0%). The above comprehensive comparison results demonstrate the effectiveness of our proposed method.

**GTEA & BEOID & ActivityNet 1.3.** We further evaluate the effectiveness and robustness of the proposed method on three other action detection benchmark datasets in Table 2. On both the GTEA and BEOID datasets, our method achieves a notable performance gain, outperforming SMBD by 2.9% and 2.8% on the average mAP(0.1:0.7), respectively. When compared to proposal-based methods, our proposal-level boundary adjustment surpasses HR-Pro by 4.0% and 3.5%. On the large-scale dataset ActivityNet 1.3, our method also achieves competitive results, with an average mAP (0.5:0.95) of 26.3%, only slightly behind SNPR's 26.5%. In addition, our method achieves 27.4% average mAP (0.1:0.7) via proposal refinement, outperforming HR-Pro (27.1%) by 0.3%.

#### 4.4. Evaluation of Temporal Consistency

Besides evaluating temporal action localization performance, we also evaluate the performance of three self-supervised tasks to measure the model's perception of temporal consistency in Table 3. In detail, we perform Gaussian sampling on the action instances from the THUMOS'14 test set, process the sampled points as described in

Section 3.3, and then input them into three task heads for performance evaluation. In the Action Completion task, the cosine similarity between the predicted snippet features and the corresponding target snippet is 99.2, and the cosine distance is 0.08, highlighting the excellent ability to predict action snippets using temporal contextual information. In the Action Order Understanding task, our order discriminator  $D_{aou}$  achieves 92.9% in AUC (Area Under the ROC Curve) for binary classification and a classification accuracy (ACC) of 85.7%, which demonstrates the model’s strong understanding of temporal action sequence order. In Action Regularity Understanding, the regularity discriminator also performed well in identifying action regularity, with an AUC of 85.9% and an accuracy of 77.4%. This also indirectly indicates that the recognition of action regularity is inherently more challenging than action order prediction.

#### 4.5. Ablation Study

We perform a set of ablation experiments in this section on THUMOS’14, as it is the most challenging dataset.

**Contribution of each components.** In Table 4, we display the action detection results of different combinations of proxy tasks. “AC”, “AOU”, and “ARU” represent our designed action completion, action order understanding, and action regularity understanding self-supervised tasks. Regarding average mAP (0.1:0.7), the baseline (Row. 1) reaches a score of only 56.2% without any proxy tasks. In the setup with only one auxiliary task, we notice that “ARU” contributes the most (Row. 4 *v.s.* Row. 1), then the “AOU” (Row. 3 *v.s.* Row. 1), and last the “AC” (Row. 2 *v.s.* Row. 1). When the number of proxy tasks increases to 2, we observe that both “AC+AOU” and “AC+ARU” achieve the same average mAP (0.1:0.7) of 57.6%, while “AOU+ARU” had a slightly lower mAP of 57.5%. With the complete set of auxiliary tasks, the performance reaches its peak, with average mAP scores of 58.2 (0.1:0.7), 69.2 (0.1:0.5), and 49.3 (0.3:0.7).

**Effectiveness of the length of temporal windows.** In Table 5, we evaluate the performance of our method using different temporal window lengths, each composed of the labeled snippet and its neighboring snippets. Both longer and shorter temporal windows can degrade the performance. This is because the longer temporal windows may introduce noise snippets (*e.g.*, background segments visually similar to actions) and the

shorter temporal windows cannot provide sufficient action information. Therefore, we set the length of the temporal window to 5 as a balanced setting.

**Influence of different feature extractors.** We study the influence of different feature extractors on the performance of our method in Table 6. When utilizing the same type of pre-trained network (*e.g.*, video swin transformer [48]), we observe that a larger scale of pre-training data (Row .4 *v.s.* Row. 3) and more fine-grained convolutions (Row .3 *v.s.* Row. 2) can boost action detection performance. I3D outperforms Video Swin because it utilizes not only RGB features but also optical flow features. VideoMAEv2 [49] obtains the best performance as it can learn strong feature representations from a vast amount of unlabeled video data, followed by further training on the K710. To make a fair comparison with previous methods, I3D is selected as the feature extractor.

**Impact of point annotations.** We conduct an ablation study to explore the influence of point annotations from different distributions on THUMOS14 in Table 7. The performance of manual annotation and uniform annotation are degraded as some points fall near the boundary regions, leading to confusion between actions and background. In contrast, center sampling performs better because it includes more salient action points, rather than the ambiguous points in the boundary regions. Gaussian-based sampling achieves the best average mAP (0.1:0.7) of 58.2 because it covers a wider range of diverse points.

#### *4.6. Further Discussion on Implementation*

##### ***How sensitive is the model performance to the weights of the auxiliary losses?***

We report numerical results on the sensitivity of model quality to auxiliary loss weights in Table 8.

Given that all three auxiliary tasks have roughly equal contributions (see Table 4 in the original paper), we simplify the configuration by assigning a shared weight  $\lambda$  to all three auxiliary tasks. For example,  $\lambda = 0.5$  means all auxiliary loss weights are 0.5.

Our experiments show that  $\lambda = 0.5$  provides the best trade-off. Increasing  $\lambda$  can dilute the main loss, while decreasing it weakens the effect of auxiliary guidance.

##### ***How much computational complexity is introduced by the auxiliary tasks?***

Table 4: Ablation study on THUMOS’14.  $\uparrow$  denotes the relative gain between our full model and baseline.

Row Index	Setup			AVG mAP@IoU(%)		
	AC	AOU	ARU	[0.1:0.5]	[0.3:0.7]	[0.1:0.7]
1				67.4	46.9	56.2
2	✓			67.5	47.5	56.6
3		✓		68.1	47.2	56.8
4			✓	68.0	47.8	56.9
5	✓	✓		68.6	48.5	57.6
6		✓	✓	68.9	48.1	57.5
7	✓		✓	68.4	49.0	57.6
8	✓	✓	✓	<b>69.2</b> $\uparrow^{1.8}$	<b>49.3</b> $\uparrow^{2.4}$	<b>58.2</b> $\uparrow^{2.0}$

Table 5: Ablation of different length of temporal windows on THUMOS’14.

Temporal Windows	mAP@IoU (%)				AVG [0.1:0.7]
	0.1	0.3	0.5	0.7	
3	83.0	71.4	49.3	23.0	57.6
5	82.5	71.5	51.4	23.3	58.2
7	81.1	70.3	49.4	22.3	56.7

Table 6: Ablation of different feature extractors on THUMOS’14.

Feature Type	Pretrain	mAP@IoU (%)				AVG [0.1:0.7]
		0.1	0.3	0.5	0.7	
I3D (default)	K400	82.5	71.5	51.4	23.3	58.2
Video Swin <sup>16x7x7</sup>	K400	79.0	65.4	45.3	19.5	53.0
Video Swin <sup>8x7x7</sup>	K400	79.8	67.4	46.3	19.7	54.0
Video Swin <sup>8x7x7</sup>	K600	80.2	67.6	46.0	19.9	54.2
VideoMAEv2	K710	84.4	76.1	55.7	25.9	61.6

Table 7: Ablation of the point-level annotations from different distributions on THUMOS’14.

Point Distribution	mAP@IoU (%)				AVG [0.1:0.7]
	0.1	0.3	0.5	0.7	
Manual	83.3	69.6	43.4	16.6	54.2
Uniform	81.6	68.1	47.4	21.4	55.5
Center	82.0	70.4	49.3	22.6	57.0
Gaussian (default)	82.5	71.5	51.4	23.3	58.2

Table 8: Effect of coefficient  $\lambda$  on average mAP@[0.1:0.7]. Here,  $\lambda$  denotes the shared weight for the three auxiliary tasks:  $\lambda_{ac} = \lambda_{aou} = \lambda_{aru}$ .

$\lambda$	0.1	0.2	0.3	0.4	0.5	0.6	0.7	0.8	0.9	1.0
mAP (%)	57.1	57.6	57.5	58.0	<b>58.2</b>	57.8	57.5	57.6	57.1	56.8

The auxiliary tasks are only active during training. During training, our model has an average computational cost of 41.70 GFLOPs per sample, slightly higher than the 39.11 GFLOPs of the baseline. At inference time, since the auxiliary branches are removed, our model has the same complexity as the baseline: 13.53 GFLOPs per sample.

***Is Action Order Understanding Task a special case of Action Regularity Understanding Task?***

No, Action Order Understanding Task uses reversed sequences as negatives, which retain temporal logic and focus on modeling action order. In contrast, the Action Regularity Understanding Task generates negative samples by randomly shuffling frames to model the difference between regular and abnormal temporal patterns. To ensure Action Order Understanding Task is not a special case of Action Regularity Understanding Task, we have filtered out reversed sequences when generating negatives for Action Regularity Understanding Task (*i.e.*, if a reversed sequence is generated, we re-shuffle it until a non-reversed order is obtained). This prevents overlap and shows the tasks are complementary.

***Why utilize cosine distance instead of L1/L2 for semantic gap evaluation?***

We use cosine similarity because the Action Completion Task predicts snippet-level features, where semantic alignment matters more than absolute differences. L1/L2 losses are more suited for pixel-level image reconstruction.

***4.7. Qualitative Results***

**Qualitative comparison.** In Figure 3, we provide a qualitative comparison of our method against LACP and HR-Pro on the test videos of ActivityNet 1.3. The results clearly show that our method generates more accurate action instance localization. Taking Figure 3 (a) as an example, LACP predicts only one incomplete action instance,

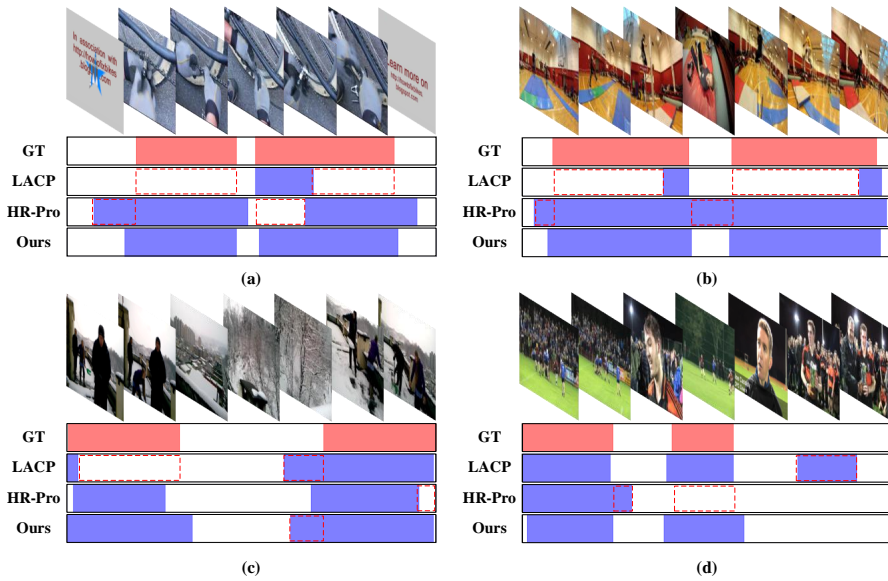


Figure 3: Qualitative comparison between our proposed method, HR-Pro [17], and LACP [7] on ActivityNet 1.3. We provide four cases of temporal action localization from different action classes, including “Fixing bicycle”, “Powerbocking”, “Shoveling snow”, and “Hurling”. Prediction errors are highlighted with red dashed boxes. The IoUs between our detection results and the ground truths are notably higher.

whereas the ground-truth annotation contains two complete action instances. While HR-Pro detects two action instances, the left prediction includes extra segments, and the right one misses part of the action. In contrast, our method not only successfully identifies all action instances but also accurately localizes their boundaries. In Figure 3 (b), LACP identifies only a small portion of the action, while HR-Pro incorrectly merges two separate actions into one, ignoring the background segment in between. By contrast, our approach accurately captures two entire action sequences. In Figure 3 (c), despite a slight over-detection in the second action instance, our method demonstrates superior overall completeness relative to the other two methods. Figure 3 (d) shows that the detection results of our method largely cover the ground truth, while LACP produces false positives and HR-Pro misses the second action instance.

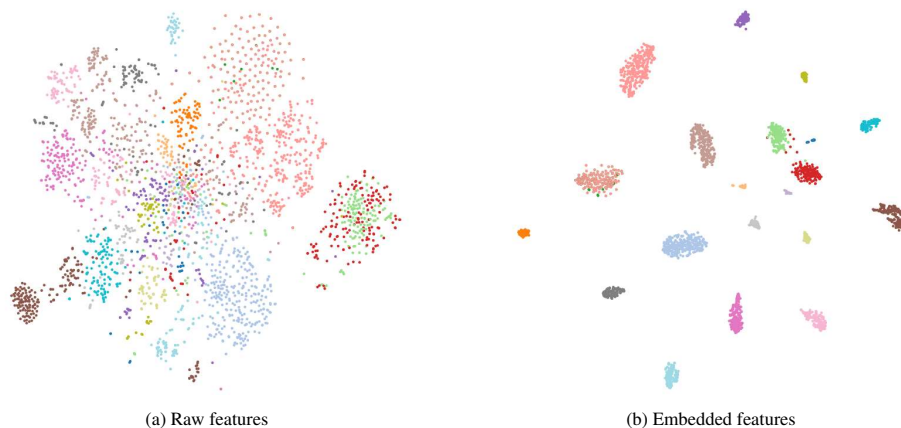


Figure 4: T-SNE visualization of the distribution of (a) raw features and (b) embedded features, respectively, where dots represent snippet features and different colors indicate different action categories.

**Feature embedding visualization.** We use T-SNE to visualize the raw features and embedded features on THUMOS’14 in Figure 4. Figure 4 (a) shows that the raw features are difficult to distinguish between different actions, but in Figure 4 (b), they form clearer clusters after training.

## 5. Conclusion

In this paper, we point out that existing methods mainly rely on point-supervised snippet classification for model training, but lack effective modeling of temporal consistency. To bridge this gap, we introduce three self-supervised tasks based on point annotations, including Action Completion, Action Order Understanding, and Action Regularity Understanding. These tasks empower the model to reason about action context, temporal order, and regularity patterns, respectively. We incorporate these tasks into the base action detection framework to jointly model temporal consistency and learn the temporal action localization. We will also make the code publicly available. Extensive experiments on four benchmark datasets demonstrate the robustness and effectiveness of our method and highlight the significant potential of point annotations for temporal action localization.

## References

- [1] Y. Ma, L. Qing, G. Li, Y. Qi, A. Beheshti, Q. Z. Sheng, Q. Huang, RETTA: retrieval-enhanced test-time adaptation for zero-shot video captioning, *Pattern Recognit.* 171 (2026) 112170.
- [2] J. Kim, M. Lee, J. Heo, Long-term pre-training for temporal action detection with transformers, *Pattern Recognit.* 171 (2026) 112144.
- [3] G. Chen, Y. Zheng, W. Zhu, J. Wang, T. Lu, Feature matters: Revisiting channel attention for temporal action detection, *Pattern Recognit.* 169 (2026) 111846.
- [4] Y. Zou, Q. Zhao, P. K. Sarker, S. Li, L. Wang, W. Liu, Diffusion-based framework for weakly-supervised temporal action localization, *Pattern Recognit.* 160 (2025) 111207.
- [5] C. Wang, J. Wang, P. Liu, Complementary adversarial mechanisms for weakly-supervised temporal action localization, *Pattern Recognit.* 139 (2023) 109426.
- [6] F. Ma, L. Zhu, Y. Yang, S. Zha, G. Kundu, M. Feiszli, Z. Shou, Sf-net: Single-frame supervision for temporal action localization, in: A. Vedaldi, H. Bischof, T. Brox, J. Frahm (Eds.), *ECCV*, Vol. 12349 of *Lecture Notes in Computer Science*, Springer, 2020, pp. 420–437.
- [7] P. Lee, H. Byun, Learning action completeness from points for weakly-supervised temporal action localization, in: *ICCV*, IEEE, 2021, pp. 13628–13637.
- [8] J. Fu, J. Gao, C. Xu, Compact representation and reliable classification learning for point-level weakly-supervised action localization, *TIP* 31 (2022) 7363–7377.
- [9] G. Li, D. Cheng, N. Wang, J. Li, X. Gao, Neighbor-guided pseudo-label generation and refinement for single-frame supervised temporal action localization, *TIP* 33 (2024) 2419–2430.
- [10] T. Lin, X. Zhao, H. Su, C. Wang, M. Yang, Bsn: Boundary sensitive network for temporal action proposal generation, in: *ECCV*, 2018, pp. 3–19.

- [11] T. Lin, X. Liu, X. Li, E. Ding, S. Wen, Bmn: Boundary-matching network for temporal action proposal generation, in: ICCV, 2019, pp. 3889–3898.
- [12] C.-L. Zhang, J. Wu, Y. Li, Actionformer: Localizing moments of actions with transformers, in: ECCV, 2022, pp. 492–510.
- [13] L. Wang, Y. Xiong, D. Lin, L. Van Gool, Untrimmednets for weakly supervised action recognition and detection, in: CVPR, 2017, pp. 4325–4334.
- [14] A. Islam, C. Long, R. J. Radke, A hybrid attention mechanism for weakly-supervised temporal action localization, in: AAAI, AAAI Press, 2021, pp. 1637–1645.
- [15] Y. Zhao, H. Zhang, Z. Gao, W. Gao, M. Wang, S. Chen, A novel action saliency and context-aware network for weakly-supervised temporal action localization, TMM 25 (2023) 8253–8266.
- [16] Z. Xia, J. Cheng, S. Liul, Y. Hu, S. Wang, Y. Zhang, L. Dang, Realigning confidence with temporal saliency information for point-level weakly-supervised temporal action localization, in: CVPR, IEEE, 2024, pp. 18440–18450.
- [17] H. Zhang, X. Wang, X. Xu, Z. Qing, C. Gao, N. Sang, Hr-pro: Point-supervised temporal action localization via hierarchical reliability propagation, in: M. J. Wooldridge, J. G. Dy, S. Natarajan (Eds.), AAAI, AAAI Press, 2024, pp. 7115–7123.
- [18] A. Kendall, Y. Gal, R. Cipolla, Multi-task learning using uncertainty to weigh losses for scene geometry and semantics, in: CVPR, Computer Vision Foundation / IEEE Computer Society, 2018, pp. 7482–7491.
- [19] O. Sener, V. Koltun, Multi-task learning as multi-objective optimization, in: S. Bengio, H. M. Wallach, H. Larochelle, K. Grauman, N. Cesa-Bianchi, R. Garnett (Eds.), NeurIPS, 2018, pp. 525–536.
- [20] D. Bhattacharjee, T. Zhang, S. Sússtrunk, M. Salzmann, Muit: An end-to-end multitask learning transformer, in: CVPR, IEEE, 2022, pp. 12021–12031.

- [21] Y. Gao, J. Ma, M. Zhao, W. Liu, A. L. Yuille, NDDR-CNN: layerwise feature fusing in multi-task cnns by neural discriminative dimensionality reduction, in: CVPR, Computer Vision Foundation / IEEE, 2019, pp. 3205–3214.
- [22] T.-Y. Lin, P. Goyal, R. Girshick, K. He, P. Dollár, Focal loss for dense object detection, in: ICCV, 2017, pp. 2980–2988.
- [23] P. Li, J. Cao, X. Ye, Prototype contrastive learning for point-supervised temporal action detection, *Expert Syst. Appl.* 213 (Part) (2023) 118965.
- [24] J. Devlin, M. Chang, K. Lee, K. Toutanova, BERT: pre-training of deep bidirectional transformers for language understanding, in: J. Burstein, C. Doran, T. Solorio (Eds.), NAACL, Association for Computational Linguistics, 2019, pp. 4171–4186.
- [25] N. Bodla, B. Singh, R. Chellappa, L. S. Davis, Soft-nms - improving object detection with one line of code, in: ICCV, IEEE Computer Society, 2017, pp. 5562–5570.
- [26] H. Idrees, A. R. Zamir, Y. Jiang, A. Gorban, I. Laptev, R. Sukthankar, M. Shah, The THUMOS challenge on action recognition for videos "in the wild", *Computer Vision and Image Understanding* 155 (2017) 1–23.
- [27] D. Damen, T. Leelasawassuk, O. Haines, A. Calway, W. W. Mayol-Cuevas, You-do, i-learn: Discovering task relevant objects and their modes of interaction from multi-user egocentric video, in: M. F. Valstar, A. P. French, T. P. Pridmore (Eds.), BMVA, BMVA Press, 2014.
- [28] A. Fathi, X. Ren, J. M. Rehg, Learning to recognize objects in egocentric activities, in: CVPR, IEEE Computer Society, 2011, pp. 3281–3288.
- [29] F. C. Heilbron, V. Escorcia, B. Ghanem, J. C. Niebles, Activitynet: A large-scale video benchmark for human activity understanding, in: CVPR, IEEE Computer Society, 2015, pp. 961–970.

- [30] J. Carreira, A. Zisserman, Quo vadis, action recognition? A new model and the kinetics dataset, in: CVPR, IEEE Computer Society, 2017, pp. 4724–4733.
- [31] C. Ju, P. Zhao, S. Chen, Y. Zhang, Y. Wang, Q. Tian, Divide and conquer for single-frame temporal action localization, in: ICCV, IEEE, 2021, pp. 13435–13444.
- [32] Z. Qing, H. Su, W. Gan, D. Wang, W. Wu, X. Wang, Y. Qiao, J. Yan, C. Gao, N. Sang, Temporal context aggregation network for temporal action proposal refinement, in: CVPR, Computer Vision Foundation / IEEE, 2021, pp. 485–494.
- [33] D. Sridhar, N. Quader, S. Muralidharan, Y. Li, P. Dai, J. Lu, Class semantics-based attention for action detection, in: ICCV, IEEE, 2021, pp. 13719–13728.
- [34] R. Zeng, W. Huang, M. Tan, Y. Rong, P. Zhao, J. Huang, C. Gan, Graph convolutional module for temporal action localization in videos, TPAMI 44 (10) (2022) 6209–6223.
- [35] C. Zhao, A. K. Thabet, B. Ghanem, Video self-stitching graph network for temporal action localization, in: ICCV, IEEE, 2021, pp. 13638–13647.
- [36] C. Lin, C. Xu, D. Luo, Y. Wang, Y. Tai, C. Wang, J. Li, F. Huang, Y. Fu, Learning salient boundary feature for anchor-free temporal action localization, in: CVPR, Computer Vision Foundation / IEEE, 2021, pp. 3320–3329.
- [37] H. Ren, W. Yang, T. Zhang, Y. Zhang, Proposal-based multiple instance learning for weakly-supervised temporal action localization, in: CVPR, IEEE, 2023, pp. 2394–2404.
- [38] J. Zhou, L. Huang, L. Wang, S. Liu, H. Li, Improving weakly supervised temporal action localization by bridging train-test gap in pseudo labels, in: CVPR, IEEE, 2023, pp. 23003–23012.
- [39] M. N. Rizve, G. Mittal, Y. Yu, M. Hall, S. Sajeev, M. Shah, M. Chen, Pivotal: Prior-driven supervision for weakly-supervised temporal action localization, in: CVPR, IEEE, 2023, pp. 22992–23002.

- [40] W. Yun, M. Qi, C. Wang, H. Ma, Weakly-supervised temporal action localization by inferring salient snippet-feature, in: M. J. Wooldridge, J. G. Dy, S. Natarajan (Eds.), *AAAI*, AAAI Press, 2024, pp. 6908–6916.
- [41] G. Lim, H. Kim, J. Kim, Y. Choi, Probabilistic vision-language representation for weakly supervised temporal action localization, in: J. Cai, M. S. Kankanhalli, B. Prabhakaran, S. Boll, R. Subramanian, L. Zheng, V. K. Singh, P. César, L. Xie, D. Xu (Eds.), *ACM MM*, ACM, 2024, pp. 5507–5516.
- [42] Q. Zhang, Y. Qi, X. Tang, R. Yuan, X. Lin, K. Zhang, C. Yuan, Rethinking pseudo-label guided learning for weakly supervised temporal action localization from the perspective of noise correction, in: T. Walsh, J. Shah, Z. Kolter (Eds.), *AAAI*, AAAI Press, 2025, pp. 10085–10093.
- [43] D. Moltisanti, S. Fidler, D. Damen, Action recognition from single timestamp supervision in untrimmed videos, in: *CVPR*, Computer Vision Foundation / IEEE, 2019.
- [44] L. Yang, J. Han, T. Zhao, T. Lin, D. Zhang, J. Chen, Background-click supervision for temporal action localization, *TPAMI* 44 (12) (2022) 9814–9829.
- [45] M. Liu, L. Wang, S. Zhou, K. Xia, Q. Wu, Q. Zhang, G. Hua, Stepwise multi-grained boundary detector for point-supervised temporal action localization, in: A. Leonardis, E. Ricci, S. Roth, O. Russakovsky, T. Sattler, G. Varol (Eds.), *ECCV*, Vol. 15065 of *Lecture Notes in Computer Science*, Springer, 2024, pp. 333–349.
- [46] S. M. Yoshida, T. Shibata, M. Terao, T. Okatani, M. Sugiyama, Action-agnostic point-level supervision for temporal action detection, *CoRR* abs/2412.21205 (2025).
- [47] M. Liu, L. Wang, S. Zhou, K. Xia, X. Sun, G. Hua, Boosting point-supervised temporal action localization through integrating query reformation and optimal transport, in: *CVPR*, Computer Vision Foundation / IEEE, 2025, pp. 13865–13875.

- [48] Z. Liu, J. Ning, Y. Cao, Y. Wei, Z. Zhang, S. Lin, H. Hu, Video swin transformer, in: CVPR, IEEE, 2022, pp. 3192–3201.
- [49] L. Wang, B. Huang, Z. Zhao, Z. Tong, Y. He, Y. Wang, Y. Wang, Y. Qiao, Video-mae V2: scaling video masked autoencoders with dual masking, in: CVPR, IEEE, 2023, pp. 14549–14560.